CARBON 53 (2013) 161–168

Available at www.sciencedirect.com

SciVerse ScienceDirect

journal homepage: www.elsevier.com/locate/carbon

The use of a carbon nanotube sensor for measuring strain by micro-Raman spectroscopy

Wei Qiu [a], Qiu Li [a], Zhen-Kun Lei [b], Qing-Hua Qin [c], Wei-Lin Deng [a], Yi-Lan Kang [a,*]

[a] Tianjin Key Laboratory of Modern Engineering Mechanics, Dept. of Mechanics, Tianjin University, Tianjin 300072, China
[b] State Key Laboratory of Structural Analysis for Industrial Equipment, Dept. of Engineering Mechanics, Dalian University of Technology, Dalian 116024, China
[c] Dept. of Engineering, Australian National University, Canberra, ACT 2601, Australia

ARTICLE INFO

Article history:
Received 7 June 2012
Accepted 18 October 2012
Available online 26 October 2012

ABSTRACT

We present a Raman spectroscopy study on a film of carbon nanotubes (CNTs) acting as a wireless sensor for measuring strain at the microscale. A model for the CNT strain sensor was proposed by evaluating the quantitative contributions of individual deformed CNTs to the entire Raman spectrum. The proposed model provides an analytical relationship between the in-plane strain components to be measured and the spectral parameters detected directly through polarized Raman tests on the CNT film sensor. Based on this model, a noncontact technique for strain measurements is developed. The experiments using this technique confirmed that the CNT strain sensor described is appropriate for measuring the in-plane strain components at the microscale by using polarized Raman spectroscopy.

1. Introduction

With the rapid development of microscale and nanoscale techniques, people are increasingly concerned about the microstructures, phenomena and mechanisms inside low-dimensional materials, devices and even living cells. To detect such information, the sensor carriers/media must be more sophisticated, more accurate and smaller. Carbon nanotubes (CNTs) could become robust sensing elements due to their superior and sensitive chemical, biological, electrical, spectral, and mechanical properties [1,2]. The potential applications of CNT sensors have attracted wide interest from both science and engineering fields [3–5].

Previously, the investigations of CNT sensors for strain measurements were generally performed by using electrical or spectral methods. For the former, the CNTs or their components were taken as electrical resistance strain gauges [6,7] because their resistances change linearly with the mean strain in some ranges [8,9]. These so-called piezoresistance effects [10,11] are induced by the coupling influences of the electromechanical properties of the CNTs themselves [12,13] and the tunnel and contact resistances between the nanotubes inside components [14–16]. It is really an effective idea to use these advanced nano materials with a classical method. Nevertheless, the test requires an additional electrical circuit, which is practically impossible on micro-scale samples or with micro-scale spatial resolution.

The other technique for characterization is by spectral methods. The previous experiments of Young et al. [17,18] and Cronin et al. [19] showed that the G (including G^+ and G^-) and G′ bands in the Raman spectra of CNTs and their components moved linearly with the external loading. Subsequently, Wagner et al. realized the uniaxial strain measurement [20,21] by using well-aligned CNTs [22,23] as sensors. Compared with the electrical method, the sensor measurement by means of spectroscopy is a wireless method with micrometer spatial

* *Corresponding author:* Fax: +86 22 8789 4001.
E-mail addresses: tju_ylkang@tju.edu.cn, tju_ylkang@yahoo.com.cn (Y.-L. Kang).
0008-6223/$ - see front matter
http://dx.doi.org/10.1016/j.carbon.2012.10.043

solution. This method has been applied effectively in the studies of some unidirectionally deforming samples such as CNT fibers [24].

However, the measurement of either the mean or uniaxial strain is insufficient because the strain is generally a second-order tensor with three (two normal and one shear) components in the in-plane case. Furthermore, among previous researches, there is still a lack of theoretical study on the modeling of a CNT sensor based on the mechanisms of both mechanics and physics. From the perspective of metrology, the analytical relationship between the test results (such as Raman data) and the measured targets (such as mechanical parameters) is the foundation of the application of any sensor.

The work presented below is a theoretical and experimental study on the use of a carbon nanotube sensor for strain measuring through micro-Raman spectroscopy. By analyzing the polarized Raman properties of CNTs, a mathematical model of the CNT strain sensor is developed. This model makes it possible to evaluate the quantitative contributions to the Raman spectrum of the deformed CNTs in arbitrary directions, and thus leads to an analytical relationship between the Raman data of the CNT sensors and the in-plane strain components to be measured. Based on this model, a technique for in-plane strain measurements, named the 'CNT Raman Strain Rosette', is introduced. Furthermore, some tests were conducted to verify the feasibility of this technique.

2. Mathematics of CNT-Raman strain sensor

In this section, a mathematical model is developed to establish the mechanism of the CNT-Raman strain sensor. To set up this model, two kernel relationships should be quantified. The first is the analytical relationship between the spectrum and the deformation of a single nanotube, and the second is that between the Raman spectral parameters of numerous stochastic CNTs obtained from the CNT film as the strain sensor and the in-plane strain components of the material/structure to be measured. The detailed analyses and derivations are given below.

2.1. Raman spectrum of a single CNT

In the polarized Raman spectrum of a single CNT, the intensity of the G′ band (denoted as **R**) depends on the angle between the axial direction (**AD**) and the polarizing direction (**PD**) [25,26]. For instance, the intensity is a function of α in the form $R(\alpha) = \kappa(\cos^2\alpha - 0.5\sin^2\alpha)^2$ when the CNT scatters non-resonantly [27] and $R(\alpha) = \kappa\cos^4\alpha$ when the CNT scatters resonantly and behaves as an antenna [28,29], where κ is a constant and α is the of the angle between **AD** and **PD**. Meanwhile, the location (viz. Raman_shift) of the G′ band is linearly sensitive to the axial deformation of the nanotube [19]. In addition, the half-width at half-maximum (HWHM) of the G′ band is treated as a constant in this study because it is insensitive to both the axial deformation and the polarized direction.

If a CNT is attached or embedded on the surface of an elastic plane (as shown in Fig. 1(a)) with its axis direction (**AD**) as θ, it deforms with this plane, and its axial deformation is similar to the strain of the plane in the θ direction, denoted as $\varepsilon(\theta)$. Actually, the strain, representing the relative deformation of a solid body induced by internal or external loading, is a symmetric second-order tensor comprising six components in a 3D space or three components in a plane [30]. As shown in Fig. 1 (b), the in-plane strain $\varepsilon(\theta)$ can be expressed as $\varepsilon(\theta) = \varepsilon_X\cos^2\theta + \varepsilon_Y\sin^2\theta - \gamma_{XY}\cos\theta\sin\theta$, where ε_X, ε_Y and γ_{XY} are the normal and shear strain components in X- and Y-directions, respectively. Furthermore, it has been proved that the axial strain of a single CNT is directly proportional to the increment of the G' band Raman_shift, $\Delta\omega_{(\theta)}$, in its Raman spectrum [19]. Hence, the relationship between $\Delta\omega_{(\theta)}$ and the three strain components for a single CNT can be written as

$$\begin{aligned}\Delta\omega_{(\theta)} &= \Psi_{Sensor}\cdot\varepsilon(\theta)\\ &= \Psi_{Sensor}\cdot(\varepsilon_X\cos^2\theta + \varepsilon_Y\sin^2\theta - \gamma_{XY}\cos\theta\sin\theta)\end{aligned} \quad (1)$$

Although Eq. (1) quantitatively defines the relationship between Raman_shift and strain, it is not appropriate for sensing strain because it is for a single CNT only and is thus difficult to extend directly to the case of multiple CNTs. In practice, however, it is feasible to prepare a thin film with CNTs dispersed stochastically on a solid surface to act as a strain sensor. Therefore, it is necessary to develop a relationship between the Raman_shift and the strain for such a thin film with numerous stochastic CNTs.

2.2. Raman spectrum of stochastic CNTs as sensors

As Fig. 2(a) shows, suppose a solid body whose strains are to be measured and a thin CNT film are bonded perfectly and therefore deform together. Inside this thin film, numerous CNTs are randomly distributed (shown in Fig. 2(b)). When the CNT film is detected by a polarized Raman spectroscope in the backscattering geometry with a polarizing direction (**PD**) of φ (shown in Fig. 2(c)), the spectrum obtained is the summation of the scattering data from all of the CNTs dispersed inside the sampling area. If the Raman data of any single CNT is denoted as I_s and the total spectrum is I_A, we have $I_A = \Sigma I_s$. The polarized Raman test can determine the parameters of the total spectrum I_A, such as the Raman_shift increment of I_A (denoted as $\Delta\Omega^{(\varphi)}$), but not those of any individual I_s. Therefore, the CNTs can be used as strain sensors when, and only when, the quantitative relationship between the properties of the total spectrum I_A and the strain components of the measured body exists.

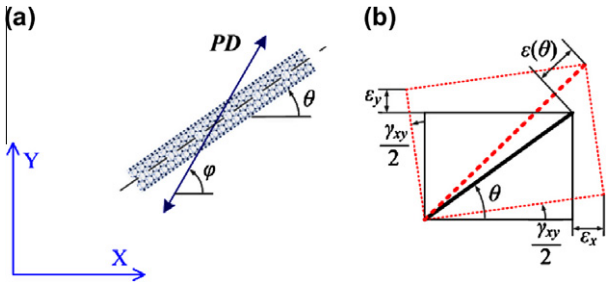

Fig. 1 – Diagrammatic sketches of (a) a single CNT fixed on a deformed plane and (b) the in-plane strain components.

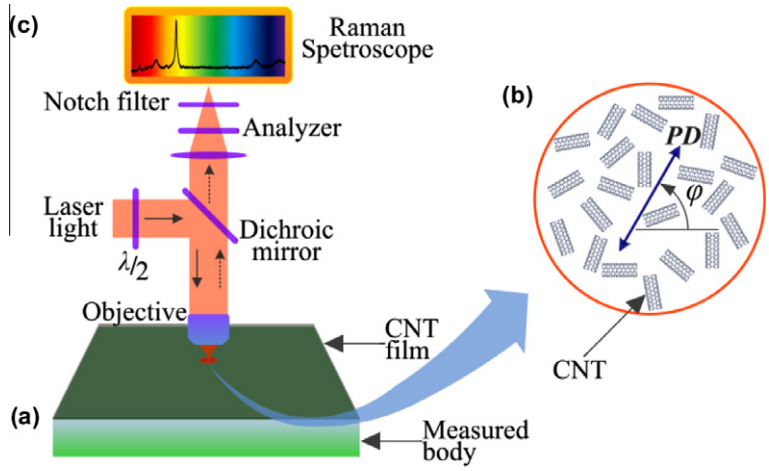

Fig. 2 – Diagrammatic sketches of CNT strain sensors characterized by polarized micro-Raman spectroscopy. (a) Measured body affixed with a CNT thin film as a strain sensor, (b) Raman sampling spot on the CNT film, where the CNTs are dispersed uniformly and stochastically in the thin film and *PD* is the polarization direction of incident light, (c) Polarized Raman spectroscope.

As mentioned above, numerous CNTs are randomly dispersed inside the sampling area of the polarized Raman microscope, and hence the nanotube population of each axial direction (*AD*) can be regarded as a constant from the perspective of statistics. Furthermore, it is reasonable to study the properties of I_A by analyzing the spectral characteristics of the CNTs with the same *AD* and then those with different *AD*s.

For those CNTs with the same *AD*, their Raman spectra should have the same intensities of G' bands regardless of the individual variances, and their Raman_shifts should also be similar, as they are under identical strain conditions. For those with different *AD*s, the spectral data of their G′ become more complex (see Fig. 3). On the one hand, the scattering intensities of the CNTs with different *AD*s are different than one another due to the antenna effect of CNT polarized Raman spectroscopy. On the other hand, the Raman_shift of the CNTs should be similar before deformation (Fig. 3(a)) but dissimilar after deformation (Fig. 3(b)) according to Eq. (1).

As the summation of the individuals, the entire spectrum has properties composed of the contributions from all of the CNTs inside the sampling spot. Without loss of generality, take the spectra of four nanotubes in the same sampling spot as example (see Fig. 4). The *AD*s of the four nanotubes are 0°/30°/60°/90° to the *PD* (viz. $\theta = \varphi$, $\varphi + 30°$, $\varphi + 60°$, $\varphi + 90°$). When the measured body is loaded by a uniaxial tension parallel to *PD*, Fig. 4 shows that the Raman_shift increment of the total spectrum $\Delta\Omega^{(\varphi)}$ is not equal to any of the Raman_shift increments of $\Delta\omega_{(\theta)}$ of any individual CNT or their arithmetic mean. Mathematically, $\Delta\Omega^{(\varphi)} \neq \Delta\omega_{(\theta)} \neq \Sigma\Delta\omega_{(\theta)}/4$ because each individual has its particular portion in the summation, inducing dissimilar contributions to the total Raman_shift increment. In another words, the Raman_shift increment of the total spectrum $\Delta\Omega^{(\varphi)}$ contains the synthetic and heterogeneous contributions of the Raman behaviors of all of the CNTs.

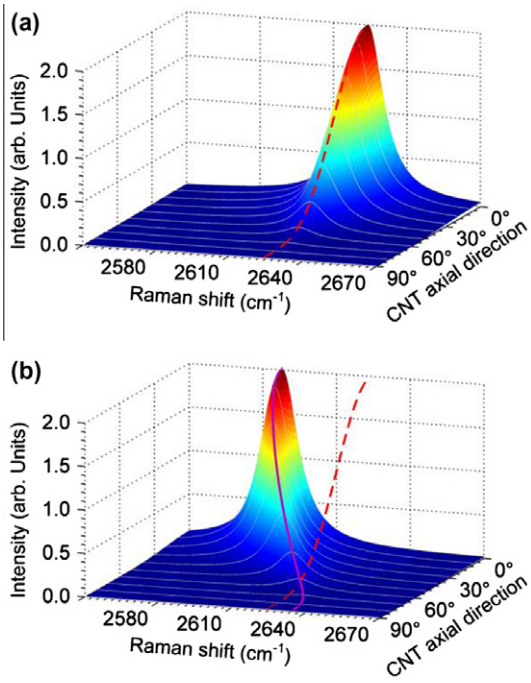

Fig. 3 – Diagrammatic sketches of the G' band polarized Raman properties of CNTs with different axial directions (a) before deformation and (b) after deformation, where the red dash line links the G' band peak locations of the CNTs with different *AD*s before deformation, and the magenta solid line links the peak locations after deformation.

2.3. *Mathematical derivation and simplification*

The contributions of individual CNTs to the total spectrum can be calculated by considering the statistical properties of a Cauchy (or normal) distribution. According to the properties

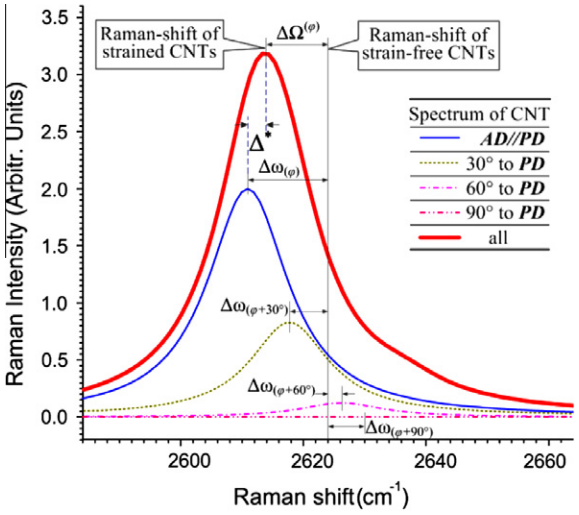

Fig. 4 – Diagrammatic sketches of the G' band Raman curves from four CNT individuals, whose axial directions (ADs) are 0°/30°/60°/90° to the polarization direction *PD*.

of a Cauchy (or normal) distribution, [31] the summation of independent Lorentzian (or Gaussian) curves is also a Lorentzian (or Gaussian) curve, and the peak location of the summed curve equals the linear accumulation of the peak locations of individual curves with their respective height gravities as weight factors, where the height gravity is the proportion of the peak height of a individual to that of the total.

It is well known that the G' band of each single CNT can be described by a Lorentzian (or Gaussian) function. Hence, the total spectrum due to all of the individuals is also a Lorentzian (or Gaussian) curve by considering the statistical properties mentioned above. Because the Raman_shift increment between the spectra of an individual CNT before and after deformation, viz. $\Delta\omega_{(\theta)}$ is given by Eq.(1), the entire Raman_shift increment in a given polarization direction (**PD**) φ, viz. $\Delta\Omega^{(\varphi)}$, can be expressed by the integral of $\Delta\omega_{(\theta)}$ as follows [32]:

$$\Delta\Omega^{(\varphi)} = \frac{\int_{\frac{-\pi}{2}}^{\frac{\pi}{2}} \Delta\omega_{(\theta)} \cdot R(\theta-\varphi)d\theta}{\int_{\frac{-\pi}{2}}^{\frac{\pi}{2}} R(\theta-\varphi)d\theta} \tag{2}$$

Substituting Eq. (1) into Eq. (2), we have

$$\Delta\Omega^{(\varphi)} = \frac{\int_{\frac{-\pi}{2}}^{\frac{\pi}{2}} \Psi_{Sensor} \cdot (\varepsilon_X \cos^2\theta + \varepsilon_Y \sin^2\theta - \gamma_{xy}\cos\theta\sin\theta) \cdot R(\theta-\varphi)d\theta}{\int_{\frac{-\pi}{2}}^{\frac{\pi}{2}} R(\theta-\varphi)d\theta} \tag{3}$$

Eq. (3) gives an analytical relationship between the in-plane strain components of the measured body and the Raman_shift increment of randomly dispersed CNTs, which defines a mathematical expression of the CNT strain sensor by considering the quantitative contribution of all of the CNTs to the entire Raman spectrum. In this relationship, ε_X, ε_Y and γ_{XY} are the measuring targets, and $\Delta\Omega^{(\varphi)}$ is detectable directly through polarized Raman system. In addition, Ψ_{Sensor} can be obtained through calibrations, and the intensity $R(\theta-\varphi)$ depends on the resonant Raman state of the CNTs. In other words, if the function of $R(\theta-\varphi)$ is determined, the in-plane strain components are measured by detecting the Raman_shift increment through polarized Raman.

The theoretical model of CNT strain sensor above can be generalized further by introducing a *distributing density function* $\rho(\theta)$, which describes the distribution density of CNTs in each axial direction θ. In other words, $\rho(\theta)$ denotes the proportion of the CNT population whose **AD** is θ to the total CNT population. With this *distributing density function*, the CNTs used as strain sensors may be dispersed stochastically or non-stochastically or even oriented. Hence, the mathematical expression becomes

$$\begin{aligned}\Delta\Omega^{\varphi} &= \frac{\int_{\frac{-\pi}{2}}^{\frac{\pi}{2}} \Delta\omega_{(\theta)} \cdot R(\theta-\varphi)\cdot\rho(\theta)d\theta}{\int_{\frac{-\pi}{2}}^{\frac{\pi}{2}} R(\theta-\varphi)d\theta} \\ &= \frac{\int_{\frac{-\pi}{2}}^{\frac{\pi}{2}} \Psi_{Sensor} \cdot \left(\varepsilon_X\cos^2\theta + \varepsilon_Y\sin^2\theta - \gamma_{xy}\cos\theta\sin\theta\right)\cdot R(\theta-\varphi)\cdot\rho(\theta)d\theta}{\int_{\frac{-\pi}{2}}^{\frac{\pi}{2}} R(\theta-\varphi)\cdot\rho(\theta)d\theta}\end{aligned} \tag{4}$$

When the polarized Raman scattering of the CNTs is in a resonant state, which means it has an antenna effect, [28] and the **PD**s of the incident and scattered light in the Raman spectroscope are controlled so that they remain constantly parallel to each other, $R = \kappa\cos^4(\theta-\varphi)$ and κ = const.; then, Eq.(3) can be simplified as

$$\begin{aligned}\Delta\Omega^{(\varphi)} &= \frac{1}{6}\Psi_{Sensor} \\ &\cdot [(3+2\cos 2\varphi)\varepsilon_X + (3-2\cos 2\varphi)\varepsilon_Y - 2\sin 2\varphi\cdot\gamma_{XY}]\end{aligned} \tag{5}$$

As a special form of Eq. (3), Eq. (5) is more suitable for strain measurement because the relationship between $\Delta\Omega^{\varphi}$ and the strain components is clearly defined this equation. Meanwhile, it is also straightforward to achieve CNT resonant Raman spectroscopy because plenty of existing theoretical and experimental reports had proved that metal single-wall carbon nanotubes (M-SWCNTs) behave as resonant Raman scatters when excited by a 632.8 nm laser [33], and the semiconductor single-wall carbon nanotubes (S-SWCNTs) are resonant scatters when excited by a 514.5 nm laser [34].

It should be noted that Eq. (3) can also be reduced to other forms under different experimental modes such as "only the **PD** of incident light is controllable" and "CNT scattering in a non-resonant state". In addition, if the CNTs are well aligned to a direction θ_0, $\rho(\theta)$ is equal to one when $\theta = \theta_0$ and zero when $\theta \neq \theta_0$, and Eq. (4) becomes

$$\begin{aligned}\Delta\Omega^{(\varphi)} &= \Psi_{Sensor}\cdot\left(\varepsilon_X\cos^2\theta_0 + \varepsilon_Y\sin^2\theta_0 - \gamma_{XY}\cos\theta_0\sin\theta_0\right) \\ &= \Psi_{Sensor}\cdot\varepsilon_{\theta_0}\end{aligned} \quad when\ \rho(\theta) = \begin{cases}1 & \theta=\theta_0\\ 0 & \theta\neq\theta_0\end{cases} \tag{6}$$

Eq. (6) shows that, when the CNTs are well aligned, the Raman_shift increment is directly proportional to the normal strain in the direction of the CNTs regardless of the polarization direction of the incident light, which is similar to the conclusion by Wagner [20,21].

3. Technique: CNT raman strain rosette

Based on the theory of the CNT strain sensor given above, a technique of in-plane strain measurement called a CNT Raman strain rosette is presented. Taking Eq. (5) as an example, it indicates that the Raman_shift increment for any given **PD** can be expressed in terms of a linear combination of three in-plane strain components with dissimilar trigonometric

functions of φ as weighting factors. Eq. (5) contains three unknown quantities, and two more equations are required to uniquely determine the three unknowns. Consequently, by considering three different **PD**s and then detecting the Raman data of these three **PD**s, we may obtain three independent equations, which can be used to determine the three strain components uniquely. This method is called the *CNT Raman strain rosette*, and the equation system is called the *CNT Raman strain rosette equation set*. For illustration, if the three **PD**s are taken as 0°/45°/90°, the 45° Raman strain rosette equation set is written as

$$\begin{cases} \varepsilon_X = \frac{1}{4\Psi_{Sensor}} \cdot \left(5\Delta\Omega^{(0)} - \Delta\Omega^{(90)}\right) \\ \varepsilon_Y = \frac{1}{4\Psi_{Sensor}} \cdot \left(5\Delta\Omega^{(90)} - \Delta\Omega^{(0)}\right) \\ \gamma_{XY} = \frac{3}{2\Psi_{Sensor}} \cdot \left(\Delta\Omega^{(0)} + \Delta\Omega^{(90)} - 2\Delta\Omega^{(45)}\right) \end{cases} \tag{7}$$

Similarly, the 120° Raman strain rosette equation set for specifying three **PD**s as 0°/120°/−120° is obtained as

$$\begin{cases} \varepsilon_X = \frac{1}{6\Psi_{Sensor}} \cdot \left[8\Delta\Omega^{(0)} - (\Delta\Omega^{(120)} + \Delta\Omega^{(-120)})\right] \\ \varepsilon_Y = \frac{1}{6\Psi_{Sensor}} \cdot \left[5(\Delta\Omega^{(120)} + \Delta\Omega^{(-120)}) - 4\Delta\Omega^{(0)}\right] \\ \gamma_{XY} = \frac{\sqrt{3}}{2\Psi_{Sensor}} \cdot \left(\Delta\Omega^{(120)} - \Delta\Omega^{(-120)}\right) \end{cases} \tag{8}$$

4. Experiments

Making use of the technique of the CNT Raman strain rosette, the theoretical model of the CNT strain sensor was validated by a series of experiments on the samples including a free-standing CNT film and CNT thin films pasted on samples.

Preparation of samples: The CNT thin film in this work comprised DGEBA-based epoxy as the matrix and approximately 0.5 wt.% single-wall CNTs (–COOH functioned, TIMESNANO Ltd.) dispersed in liquid epoxy by the ultrasonic approach (24 h). The cured film had a Young's modulus of 2.00 GPa and a Poisson ratio of 0.379.

Three kinds of samples were prepared, denoted as *specimens* A, B and C. *Specimen* A was a free-standing CNT thin film approximately 160 μm thick, cut into strips of approximately 40 mm × 2 mm. *Specimen* B was a PVC (polyvinyl chloride) sheet 400 μm thick, cut into the dog-bone shape shown in Fig. 5a. A circular hole was punched in the middle of the dog-bone-shaped sample. A CNT thin film that was 30 μm thick to be used as a Raman-strain gauge was pasted on the PVC surface. Specimen C (shown in Fig. 6a) is a fiber-reinforced epoxy bar whose dimensions are $32 \times 6 \times 2$ mm^3. The unidirectional carbon fiber (Toray M40JB-12 k) is parallel to the length-direction (viz. X direction). A slot, approximately 0.8 mm wide and 2 mm tall normal to the X direction, was prepared at the middle of one longitudinal side of the bar. Then, a CNT film that was 30 μm thick was prepared on the epoxy bar surface.

Experiments: *Specimen* A was uniaxially stretched step-by-step in a mini-tensile machine with the loading direction (X direction) parallel to the longitudinal side of the specimen. A Renishaw InVia Raman spectroscope with a He–Ne laser source (632.8 nm, 2 mW) was utilized, and the incident beam was focused on the CNT film surface of each specimen in the backscattering geometry through a 50× objective lens, forming a sampling spot of approximately 2 μm in diameter. Under each loading step, a 45° Raman strain rosette was employed by recording the Raman spectra (2450–2800 cm^{-1}) of the same sampling spot for 0°/45°/90° **PD**s.

In the test on *Specimen* B, the sample was elongated uniaxially to an average strain of $\varepsilon_0 = 0.33\%$ around the middle of the dog-bone sample. After waiting for one hour for stress relaxation, a quarter of the area around the hole (shown in Fig. 5b) was scanned by the same Raman system using a 60 μm mapping step. At each of the sampling spots during Raman mapping, the 45° Raman strain rosette was applied. *Specimen C* was four-point bend loaded to a 300 μm maximum deflection. An area next to the rectangle tip of the slot (shown in Fig. 6b) was scanned with a 50 μm step length using the 45° Raman strain rosette at each spot.

All of the raw spectra were fitted by a Lorentzian function to achieve the Raman_shifts of the G′ band, which are assumed to be solely from the CNTs because both epoxy and PVC are Raman-inactive to strain and have no Raman mode between 2450 cm^{-1} and 2800 cm^{-1}.

5. Results and discussion

Fig. 7 shows the experimental data of the uniaxial tensile test on the free-standing CNT film (*Specimen* A). With the increase of the tensile loading, the Raman_shifts for different **PD**s ($\Omega^{(0)}$, $\Omega^{(45)}$ and $\Omega^{(90)}$) start from approximately 2624 cm^{-1}, change linearly before $\varepsilon_X < 0.8\%$ and then vary nonlinearly until the film breaks. The slopes in the range of linearity, $\Delta\Omega^{(0)}/\varepsilon_X$, $\Delta\Omega^{(45)}/\varepsilon_X$ and $\Delta\Omega^{(90)}/\varepsilon_X$, are −14.0, −5.9 and 2.6, respectively. By dividing the two sides of each equation in Eq. (7),

$$\begin{cases} 1 = \frac{1}{4\Psi_{Sensor}} \cdot \left(5\frac{\Delta\Omega^{(0)}}{\varepsilon_X} - \frac{\Delta\Omega^{(90)}}{\varepsilon_X}\right) \\ -\upsilon = \frac{\varepsilon_Y}{\varepsilon_X} = \frac{1}{4\Psi_{Sensor}} \cdot \left(5\frac{\Delta\Omega^{(90)}}{\varepsilon_X} - \frac{\Delta\Omega^{(0)}}{\varepsilon_X}\right) \\ \frac{\gamma_{XY}}{\varepsilon_X} = \frac{3}{2\Psi_{Sensor}} \cdot \left(\frac{\Delta\Omega^{(0)}}{\varepsilon_X} + \frac{\Delta\Omega^{(90)}}{\varepsilon_X} - 2\frac{\Delta\Omega^{(45)}}{\varepsilon_X}\right) \end{cases} \tag{9}$$

and then substituting the Raman_shift slopes and their respective **PD**s, we obtained

$$\Psi_{Sensor} = -1815.0 \text{ cm}^{-1}, \quad \upsilon = -\frac{\varepsilon_Y}{\varepsilon_X} = 0.372, \quad \frac{\gamma_{XY}}{\varepsilon_X} = 3.3\% \tag{10}$$

Eq. (10) shows that the strain-Raman_shift coefficient of the CNT sensor Ψ_{Sensor} is −1815.0 cm^{-1}, which is much higher than most of Raman-active materials (such as that of *Kevlar*-29 aramid fiber, which is 285.7 cm^{-1} [35]; SiC monofilament, which is 260 cm^{-1} [36]; and Technora fiber, which is 360 cm^{-1} [37]). Meanwhile, the Poisson ratio obtained by using the CNT Raman Strain Rosette is 0.372, which is almost equal to the true values of the thin film, 0.379. Meanwhile, the shear strains γ_{XY} compared with ε_X are nearly zero, which is congruent with the actual strain state under uniaxial tensile loading.

Fig. 5 gives the strain distributions around the circular hole under uniaxial tensile loading, where Fig. 5c–e are the CNT Raman Strain Rosette results of $\varepsilon_r/\varepsilon_0$, $\varepsilon_\theta/\varepsilon_0$ and $\gamma_{r\theta}/\varepsilon_0$, respectively, and Fig. 5f–h are their corresponding theoretical solutions [30]. The experimental results are similar to their theoretical counterparts in both the trend and the magnitude. For instance, the obtained stress concentration factor of σ_θ (viz. the maximum of $\varepsilon_\theta/\varepsilon_0$) is 2.66, approaching its theoretical value of 3. The parameter $\tau_{r\theta}$ shows a clear saddle shape symmetric about a line along $\theta = 45°$. In fact, the direct measurement of $\tau_{r\theta}$

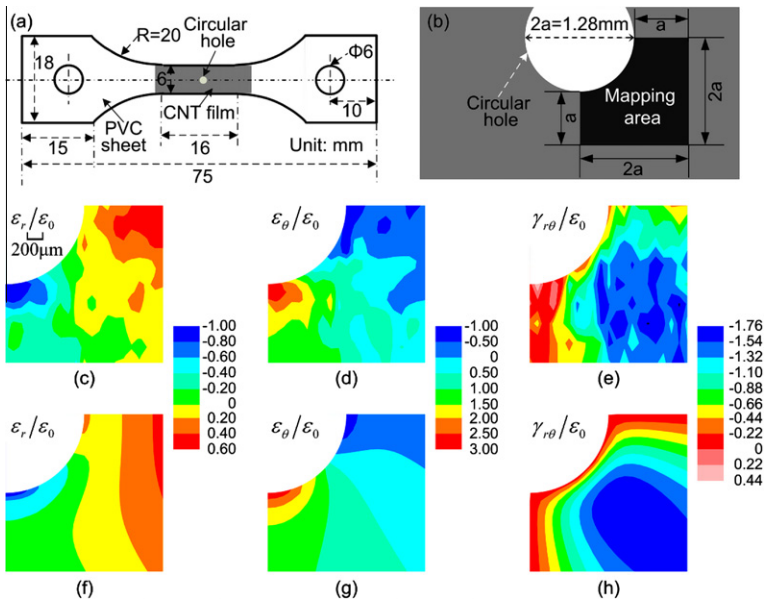

Fig. 5 – The experiments on the dog-bone PVC sheet with a circular hole (*Specimen B*) under uniaxial tensile loading. (a) The geometrical shape and dimensions, (b) Raman mapping region, (c)–(e) show the distributions of $\varepsilon_r/\varepsilon_0$, $\varepsilon_\theta/\varepsilon_0$ and $\gamma_{r\theta}/\varepsilon_0$, respectively, achieved by using the CNT Raman Strain Rosette. (f)–(h) show $\varepsilon_r/\varepsilon_0$, $\varepsilon_\theta/\varepsilon_0$ and $\gamma_{r\theta}/\varepsilon_0$, respectively, given by elastic mechanics theory.

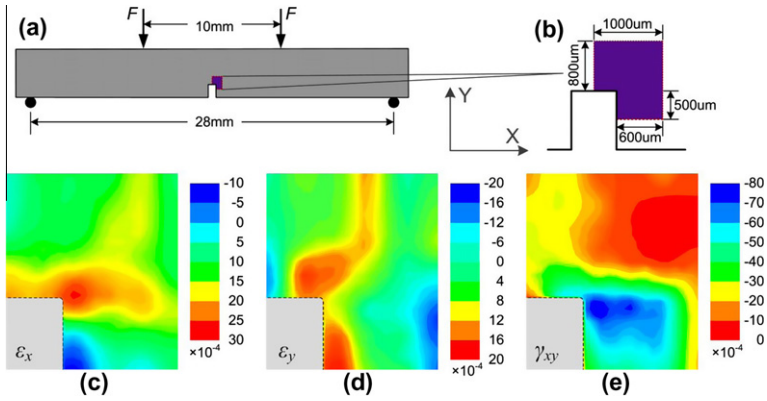

Fig. 6 – The experiments on the fiber-reinforced epoxy bar under four-point bend loading. (a) The geometrical shape, dimensions and loading type, (b) Raman mapping region, (c)–(e) the distributions of ε_x, ε_y and γ_{xy}, respectively, near the vicinity of the slop tip achieved by Raman Strain Rosette.

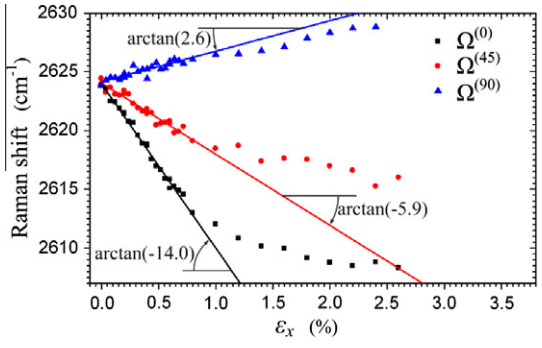

Fig. 7 – The experimental data of the uniaxial tensile test on the free-standing CNT film (*Specimen A*).

distribution at the microscale is scarcely possible by most of the experimental methods.

The experimental results on the fiber-reinforced epoxy bar with four-point bend loading are shown in Fig. 6. Non-uniform deformations exist near the vicinity of the slop tip. Particularly, the normal-strain in the either X or Y direction (Fig. 6c and d) varies from tension to compression rapidly. Meanwhile, the shear zone (Fig. 6e) is parallel to the fiber direction, neither the slope direction nor the 45° direction, which shows the specific mechanical behavior of unidirectionally fiber-reinforced materials.

The analysis above indicates that the measurement results of the CNT Raman Strain Rosette are in good agreement with the actual values, which confirms that the CNT strain sensor in this work is appropriate for detecting the in-plane strain components of a measured body accurately. Its

precision is independent of both the loading condition and the measuring direction because the mathematical model of the strain sensor calculates the Raman data from all of the CNTs in every direction. In contrast, among the previous works,[20–23] the Raman data from the *AD≠PD* CNTs are always ignored, and only those from the **AD‖PD** CNTs (viz. whose axial direction is parallel to the polarizing direction) are counted because they are dominant in the total spectrum due to the antenna effect of CNTs in polarized Raman scattering.[28,29] In this case, the corresponding Raman_shift increment is directly proportional to the normal strain in the same direction as the **PD** in the following form:

$$\Delta\Omega^{(\varphi)} = \Psi_W \cdot \varepsilon_W^{\varphi} \tag{11}$$

In Eq. (11), Ψ_W is the *strain-Raman_shift coefficient* calibrated through uniaxial tensile testing, and ε_W^{φ} is the measured value of the normal strain in the φ direction.

Eq. (11), neglecting the scatterings from the CNTs that are not parallel to the **PD,** is rational when, and only when, the CNTs are well aligned in the φ direction, which is applicable for measuring the strain in the φ direction only. Otherwise, each individual of the randomly dispersed CNTs contributes to the total spectrum, and none can be neglected. Without loss of generality, consider the Raman spectra of four CNTs whose **ADs** are 0°/30°/60°/90° to the **PD**. Fig. 4 shows that, even though the data (thin blue line) from the nanotube ***AD‖PD*** is dominant in the total spectrum (thick red line), there is a distinct distance Δ^* between the Raman_shift of the CNT parallel to the **PD** and that of all CNTs, which demonstrates that the Raman_shift induced from the CNTs that are not parallel to the **PD** is not negligible. Errors may be induced in the measured results due to Δ^* except for the loading condition, where Ψ_W is calibrated accordingly. Therefore, Eq. (11) is an approximate expression for the Raman_shift increment, and, in general, it can provide acceptable results for limiting cases only. For example, consider the experiment on *Specimen A* in this work (Fig. 7), where the measured result for the Poisson ratio obtained by the CNT Raman Strain Rosette is 0.379, which is close to the actual value, 0.372. In contrast, Eq. (11) gives the Poisson ratio $\nu = -\varepsilon_Y/\varepsilon_X = -\Delta\Omega^{(90)}/\Delta\Omega^{(0)}$=2.6/14 = 0.186, which is far from the actual value of 0.372 and obviously unacceptable.

6. Conclusions

This paper presents a theoretical and experimental study on the CNT sensor applicable for the measurement of in-plane strain components at the microscale by micro-Raman spectroscopy. In particular, the following advances have been achieved.

A theoretical model of the CNT strain sensor is achieved to build an analytical relationship between the in-plane strain components of the measured body and the Raman_shift increment of randomly dispersed CNTs. The model calculates the quantitative contribution of deformed CNTs in any direction to the entire Raman spectrum by applying the polarized Raman properties of the CNT and the statistical properties of the Cauchy (or normal) distribution.

Based on the model of the CNT strain sensor, a new wireless technique called the CNT Raman Strain Rosette is developed. The technique is applicable to measure the in-plane strain components (including the normal and shear strains) at the microscale by means of detecting the Raman_shift increments in three different polarization directions and using the corresponding CNT Raman Strain Rosette equation set.

The experiments using the CNT Raman Strain Rosette and further discussion contrasting the previous methods confirm that the CNT strain sensor is appropriate for detecting the in-plane strain components of a measured body easily and accurately, and its precision is independent of both the loading condition and the measurement direction.z

Acknowledgements

This work is financially supported by the National Basic Research Program of China (No. 2012CB937500) and the NSFC of China (Grant Nos. 11227202, 11272232, 11002097 and 10972047) and Doctoral Fund of Ministry of Education of China (No. 20090032120008).

REFERENCES

[1] Dai HJ. Carbon nanotubes: synthesis, integration, and properties. Acc Chem Res 2002;35(12):1035–44.
[2] Terrones M. Science and technology of the twenty-first century: synthesis, properties and applications of carbon nanotubes. Annu Rev Mater Res 2003;33:419–501.
[3] Wood JR, Zhao Q, Frogley MD, Meurs ER, Prins AD, Peijs T, et al. Carbon nanotubes: from molecular to macroscopic sensors. Phys Rev B 2000;62(11):7571–5.
[4] Thostenson ET, Ren ZF, Chou TW. Advances in the science and technology of carbon nanotubes and their composites: a review. Compos Sci Technol 2001;61(13):1899–912.
[5] Li C, Thostenson ET, Chou TW. Sensors and actuators based on carbon nanotubes and their composites: a review. Compos Sci Technol 2008;68(6):1227–49.
[6] Chang NK, Su CC, Chang SH. Fabrication of single-walled carbon nanotube flexible strain sensors with high sensitivity. Appl Phys Lett 2008;92(6):063501.
[7] Li X, Levy C, Elaadil L. Multiwalled carbon nanotube film for strain sensing. Nanotechnology 2008;19(4):045501.
[8] Hu N, Karube Y, Arai M, Watanabe T, Yan C, Li Y, et al. Investigation on sensitivity of a polymer/carbon nanotube composite strain sensor. Carbon 2010;48(3):680–7.
[9] Dharap P, Li ZL, Nagarajaiah S, Barrera EV. Nanotube film based on single-wall carbon nanotubes for strain sensing. Nanotechnology 2004;15(3):379–82.
[10] Oliva-Aviles AI, Aviles F, Sosa V. Electrical and piezoresistive properties of multi-walled carbon nanotube/polymer composite films aligned by an electric field. Carbon 2011;49(9):2989–97.
[11] Zhu S, Chung DDL. Analytical model of piezoresistivity for strain sensing in carbon fiber polymer-matrix structural composite under flexure. Carbon 2007;45(8):1606–13.
[12] Hartman AZ, Jouzi M, Barnett RL, Xu JM. Theoretical and experimental studies of carbon nanotube electromechanical coupling. Phys Rev Lett 2004;92(23):236804.
[13] Chen YR, Weng CI. Electronic properties of zigzag carbon nanotubes under uniaxial strain. Carbon 2007;45(8):1636–44.
[14] Huang J, Wang B, Lahiri I, Gupta AK, Eklund PC, Choi W. Tuning electrical conductance of serpentine single-walled

carbon nanotubes. Adv Funct Mater 2010 Dec 21;20(24):4388–93.
[15] Wang LH, Ding TH, Wang P. Influence of carbon black concentration on piezoresistivity for carbon-black-filled silicone rubber composite. Carbon 2009;47(14):3151–7.
[16] Hu N, Karube Y, Yan C, Masuda Z, Fukunaga H. Tunneling effect in a polymer/carbon nanotube nanocomposite strain sensor. Acta Mater 2008 Aug;56(13):2929–36.
[17] Cooper CA, Young RJ, Halsall M. Investigation into the deformation of carbon nanotubes and their composites through the use of Raman spectroscopy. Composites Part A 2001;32(3–4):401–11.
[18] Lucas M, Young RJ. Effect of uniaxial strain deformation upon the Raman radial breathing modes of single-wall carbon nanotubes in composites. Phys Rev B 2004;69(8):085405.
[19] Cronin SB, Swan AK, Unlu MS, Goldberg BB, Dresselhaus MS, Tinkham M. Resonant Raman spectroscopy of individual metallic and semiconducting single-wall carbon nanotubes under uniaxial strain. Phys Rev B 2005;72(3):035425.
[20] Zhao Q, Wood JR, Wagner HD. Stress fields around defects and fibers in a polymer using carbon nanotubes as sensors. Appl Phys Lett 2001;78(12):1748–50.
[21] Frogley MD, Zhao Q, Wagner HD. Polarized resonance Raman spectroscopy of single-wall carbon nanotubes within a polymer under strain. Phys Rev B 2002;65(11):113413.
[22] Zhao Q, Frogley MD, Wagner HD. Direction-sensitive strain-mapping with carbon nanotube sensors. Compos Sci Technol 2002;62(1):147–50.
[23] Zhao Q, Wagner HD. Two-dimensional strain mapping in model fiber-polymer composites using nanotube Raman sensing. Composites Part A 2003;34(11):1219–25.
[24] Gao Y, Li JZ, Liu LQ, Ma WJ, Zhou WY, Xie SS, et al. Axial compression of hierarchically structured carbon nanotube fiber embedded in epoxy. Adv Funct Mater 2010;20(21):3797–803.
[25] Dresselhaus MS, Dresselhaus G, Saito R, Jorio A. Raman spectroscopy of carbon nanotubes. Phys Rep 2005;409(2):47–99.
[26] Duesberg GS, Loa I, Burghard M, Syassen K, Roth S. Polarized Raman spectroscopy on isolated single-wall carbon nanotubes. Phys Rev Lett 2000;85(25):5436–9.
[27] Gommans HH, Alldredge JW, Tashiro H, Park J, Magnuson J, Rinzler AG. Fibers of aligned single-walled carbon nanotubes: polarized Raman spectroscopy. J Appl Phys 2000;88(5):2509–14.
[28] Saito R, Dresselhaus G, Dresselhaus MS. Physical properties of carbon nanotubes. London: Imperial College Press; 1998.
[29] Fantini C, Pimenta MA, Dantas MSS, Ugarte D, Rao AM, Jorio A, et al. Micro-Raman investigation of aligned single-wall carbon nanotubes. Phys Rev B 2001;63(16):161405.
[30] Love AEH. A treatise on the mathematical theory of elasticity. 4th ed. New York, USA: Dover Publications; 1944.
[31] Derman C, Gleser LJ, Olkin I. A guide to probability theory and application. New York, USA: Holt; 1973.
[32] Qiu W, Kang Y-L, Lei Z-K, Qin Q-H, Li Q. A new theoretical model of carbon nanotube strain sensor. Chin Phys Lett 2009;26(8):080701.
[33] Pimenta MA, Marucci A, Empedocles SA, Bawendi MG, Hanlon EB, Rao AM, et al. Raman modes of metallic carbon nanotubes. Phys Rev B 1998;58(24):R16016–9.
[34] Jorio A, Dresselhaus G, Dresselhaus MS, Souza M, Dantas MSS, Pimenta MA, et al. Polarized Raman study of single-wall semiconducting carbon nanotubes. Phys Rev Lett 2000;85(12):2617–20.
[35] Lei ZK, Qiu W, Kang YL, Gang L, Yun H. Stress transfer of single fiber/microdroplet tensile test studied by micro-Raman spectroscopy. Composites Part A 2008;39(1): 113–8.
[36] Ward Y, Young RJ, Shatwell RA. Application of Raman microscopy to the analysis of silicon carbide monofilaments. J Mater Sci 2004;39(22):6781–90.
[37] Prasithphol W, Young RJ. Interfacial micromechanics of technora fibre/epoxy composites. J Mater Sci 2005;40(20):5381–6.